

Strain-induced Fermi contour anisotropy of GaAs 2D holes

J. Shabani,¹ M. Shayegan,¹ and R. Winkler²

¹*Department of Electrical Engineering, Princeton University, Princeton, NJ 08544, USA*

²*Department of Physics, Northern Illinois University, DeKalb, IL 60115, USA*

(Dated: April 25, 2019)

We report measurements of magneto-resistance commensurability peaks, induced by a square array of anti-dots, in GaAs (311)A two-dimensional holes as a function of applied in-plane strain. The data directly probe the shapes of the Fermi contours of the two spin subbands that are split thanks to the spin-orbit interaction and strain. The experimental results are in quantitative agreement with the predictions of accurate energy band calculations, and reveal that the majority spin-subband has a severely distorted Fermi contour whose anisotropy can be tuned with strain.

PACS numbers: 73.23.Ad, 72.25.Dc, 71.70.Ej

Manipulation of the spin-orbit coupling and the resulting spin-splitting in two-dimensional (2D) carrier systems is of considerable current interest [1]. Such systems are the basis for novel spintronic devices [2, 3] and also allow studies of fundamental phenomena such as various phases that the 2D carriers acquire in mesoscopic structures [4, 5, 6], and the spin Hall effect [7]. An important problem is the ballistic transport of the carriers in these systems and, in particular, the ability to resolve and manipulate such transport for the two spin-subbands. Measurements of the commensurability oscillations [8] and, more recently, magnetic focusing [9], have indeed revealed spin-resolved ballistic transport in GaAs 2D hole systems (2DHSs). Here we report spin-resolved ballistic transport measurements in GaAs 2DHSs as a function of applied in-plane strain. Together with the results of our energy band calculations, the data reveal a strong distortion of the spin-subband Fermi contours with strain, especially for the majority subband. Such distortion could find use in ballistic spintronic devices that rely on the spatial separation of carriers with different spin [9].

Figure 1 captures the essence of our study. In Fig. 1(a) we show the calculated Fermi contours of the heavy and light heavy-hole (HHh and HHl) spin-subbands for a GaAs (311)A 2DHS at different values of strain (ϵ) applied along the $[01\bar{1}]$ direction. There is a severe distortion of the contours, especially for the HHh band, as a function of strain. Such distortions have been theoretically reported previously but experimental evidence has been only through piezo-resistance measurements which qualitatively agree with the calculations [10, 11]. In our study, we perforated the 2DHS with anti-dot (AD) lattices, and measured its magneto-resistance (MR) in an L-shaped Hall bar mesa. In the AD lattice, the carriers move along real-space cyclotron trajectories with orbit shapes that are similar to the shape of the Fermi contour in reciprocal space but are rotated by 90° . When these orbits become “commensurate” with the AD lattice period, the MR exhibits a peak [12, 13, 14, 15, 16, 17, 18]. The primary (smallest) such orbits are shown in Fig. 1(b) for the HHh and HHl holes for the current parallel to the

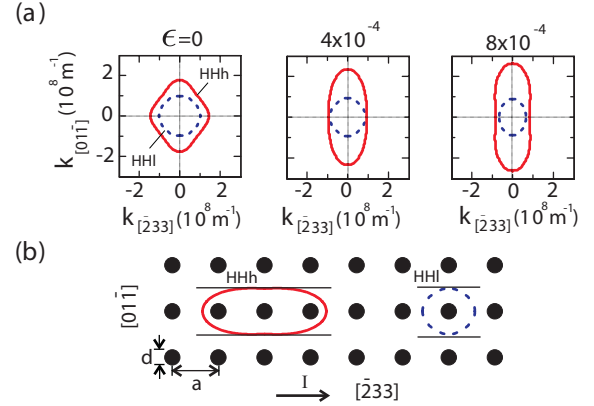


FIG. 1: (Color online) (a) Calculated Fermi contours for the HHh and HHl bands of GaAs (311)A 2D holes at $p = 2.45 \times 10^{11} \text{ cm}^{-2}$ at the indicated strain (ϵ) values. (b) The primary commensurate orbits for the HHh and HHl bands for $\epsilon = 5 \times 10^{-4}$ for current along $[\bar{2}33]$ (see text).

$[01\bar{1}]$ direction. The MR peaks measured along $[01\bar{1}]$ and $[\bar{2}33]$ should then reveal direct information regarding the size and shape of the HHh and HHl contours. Here we provide such MR data and compare them with the peak positions expected from the calculated Fermi contours.

Our sample was grown on a GaAs (311)A substrate by molecular beam epitaxy and contains a modulation-doped 2DHS confined to a GaAs/AlGaAs heterojunction. The $\text{Al}_{0.35}\text{Ga}_{0.65}\text{As}/\text{GaAs}$ interface is 100 nm below the surface and is separated from a 17 nm-thick Si-doped $\text{Al}_{0.35}\text{Ga}_{0.65}\text{As}$ layer by a 30 nm $\text{Al}_{0.35}\text{Ga}_{0.65}\text{As}$ spacer layer. The 2DHS has a typical low temperature mobility of $1 \times 10^5 \text{ cm}^2/\text{Vs}$ along $[01\bar{1}]$ and $4.3 \times 10^5 \text{ cm}^2/\text{Vs}$ along $[\bar{2}33]$ at a 2D hole density, p , of $2.9 \times 10^{11} \text{ cm}^{-2}$. We fabricated an L-shaped Hall bar, with its arms along $[01\bar{1}]$ and $[\bar{2}33]$, via optical photo-lithography. We then deposited a layer of PMMA and patterned the square AD arrays using electron beam lithography. The AD pattern was etched to a depth of $\simeq 50 \text{ nm}$; this depth is sufficiently large to strip the dopant layer and thus deplete the holes in the AD regions, but small enough to avoid introduc-

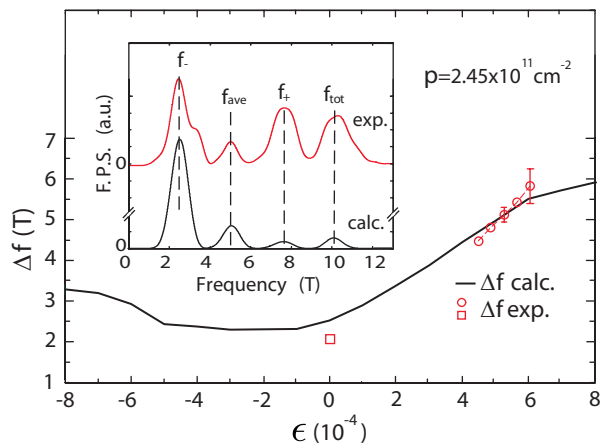


FIG. 2: (Color online) The solid curve shows $\Delta f (= f_+ - f_-)$, determined from the calculated magneto-oscillations, as a function of strain. The circles are the experimentally measured Δf . The square is the Δf measured on a sample from the same wafer not mounted on a piezo. The inset shows the Fourier power spectra (F.P.S.) of the measured and calculated magneto-oscillations at $\epsilon = 5.3 \times 10^{-4}$.

ing non-uniform strain in the AD lattice. In our sample there are two AD lattice regions, with periods $a = 600$ and 750 nm, patterned on the $[01\bar{1}]$ arm of the Hall bar, and two similar AD lattices, patterned on the $[\bar{2}33]$ arm. The ratio d/a for each AD cell is $\simeq 1/3$, where d is the AD diameter. The sample was thinned to $\simeq 200$ μm and then glued to one side of a commercial piezo-electric stack actuator with the sample's $[01\bar{1}]$ crystal direction aligned to the piezo's poling direction. Voltage biasing the piezo results in in-plane strain which is transmitted to the sample [19, 20]. We specify strain (ϵ) values along the poling direction; in the perpendicular ($[\bar{2}33]$) direction, the strain is approximately -0.38ϵ [19]. Longitudinal MR was measured, as a function of perpendicular magnetic field (B) at $T = 0.3$ K. The data reported here were all taken during a single sample cool-down.

Before presenting the commensurability MR data we first discuss our measurements of spin-splitting which we use to determine the amount of residual (built-in) strain in our sample. This residual strain exists because of the anisotropic contraction of the piezo-actuator to which the sample is glued, and depends on the cool-down of the piezo and the sample. We determine this strain by comparing the measured spin-splitting in our sample to the results of our self-consistent calculations of 2D hole bands, based on the 8×8 Kane Hamiltonian and augmented by the strain Hamiltonian of Bir and Pikus [1, 21, 22]. They take into account the spin-orbit coupling due to both the structure inversion asymmetry of the GaAs/AlGaAs heterojunction as well as the bulk inversion asymmetry of the underlying zinc-blende structure [23]. These energy band calculations have successfully explained the spin-orbit induced spin-splitting

and its dependence on density, electric field and strain in 2DHSs [8, 20, 24]. To make a direct comparison with the experimental data, we calculated the Landau fan chart as a function of B and determined the magneto-oscillations of the density of states at the Fermi energy [1, 25]. We then calculated the Fourier power spectrum of these oscillations and obtained the frequencies f_+ and f_- that correspond to the majority (HHh) and minority (HHl) spin-subbands. An example of such a spectrum is shown in the inset of Fig. 2 (lower trace). The difference Δf between f_+ and f_- is a measure of spin-splitting and can be directly compared to the experimentally determined Δf which we obtain from the Fourier transform of the measured Shubnikov-de Haas (SdH) oscillations; the upper trace in Fig. 2 inset shows such a spectrum.

In Fig. 2 we show the calculated Δf (solid curve) as a function of ϵ . We emphasize that the calculations were done based on the sample structure and there are no fitting parameters. In this plot we have also included a point (open square) from SdH oscillations measured on a sample from the same wafer which was not mounted on a piezo and is therefore free of strain. This data point agrees well with the calculations. In Fig. 2 we also plot Δf , determined from the SdH oscillations measured in the unpatterned regions of the piezo-mounted sample (open circles), where we have shifted all the measured data points horizontally by 5.7×10^{-4} in order to match the calculated Δf . (Note that the relative strains for these data points are determined from our calibration of the piezo-actuator, and are known to better than about 10%.) The plot of Fig. 2 implies that the sample is under $\simeq 5.7 \times 10^{-4}$ of residual (tensile) strain. This is somewhat larger than the typical residual strain values in our experiments on other samples, but is not unreasonable. In the remainder of this report, we assume that this is indeed the residual strain in our sample.

We now describe the results of our low-field MR measurements on the AD lattice regions of the sample. First we focus on the results for the $a = 600$ nm period region with the current along $[01\bar{1}]$. The MR traces for this region are shown in Fig. 3(a) for different values of strain as indicated. We observe two strong MR peaks, labelled as A and B in the figure. The field positions of these peaks (B_P) are plotted in Fig. 3(a') for different values of ϵ . Note that these strain values are based on Fig. 2 data, i.e., a residual strain of 5.7×10^{-4} is assumed, but otherwise there are no adjustable parameters. The data of Figs. 3(a) and (a') indicate that peak A moves to higher fields as the sample is further strained while peak B shifts to slightly smaller fields. As we discuss below, the positions of these peaks and their dependence on strain are in excellent agreement with what we expect from our calculations of our sample's Fermi contours.

Examples of the calculated HHh and HHl spin-subband Fermi contours are shown in Fig. 1(a). When the cyclotron orbit diameter in the direction perpendicular to

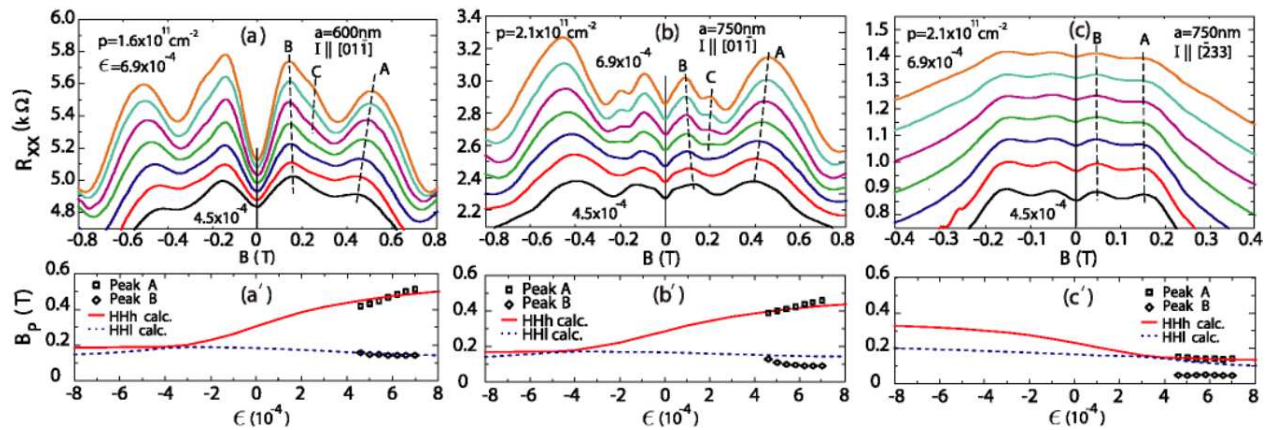


FIG. 3: (Color online) (a),(b) and (c): Low-field magneto-resistance traces for the indicated 2D hole density (p), anti-dot lattice period (a), and current direction. In each figure traces are shown for the indicated strain values from 6.9×10^{-4} (top trace) to 4.5×10^{-4} (bottom trace) in steps of 4×10^{-5} . The resistance scale is for the lowest trace and the other traces are offset vertically for clarity. (a'),(b') and (c'): Comparison of the expected magneto-resistance peak positions (B_P) based on Fermi contour calculations and the positions of the experimentally observed peaks A and B.

the current flow equals an integer multiple of the AD lattice period in that direction, the MR exhibits a peak [12, 13, 14, 15, 16, 17, 18]. In other words, we expect MR peaks at fields $B_P = 2\hbar k_F / eai$ where k_F is the Fermi wavevector along the current direction and $i = 1, 2, 3, \dots$ is an integer. In Fig. 1(b) we show the smallest ($i = 1$) commensurability orbits for the HHh and HHI holes that are expected to lead to a MR peak for the current along $[01\bar{1}]$. In Fig. 3(a') we have plotted (solid and dashed curves) the positions of the MR peaks for these two orbits expected from the calculations. Obviously, there is an excellent agreement between the expected peak positions and the experimentally observed values. This agreement is particularly remarkable considering that, except for assuming a residual strain of 5.7×10^{-4} , there are no adjustable parameters in comparing the MR peak positions.

We note that in our calculations the anisotropy of the Fermi contours emerges as follows. In hole systems the spin-splitting is greatly influenced by the energy separation between the heavy- and light-hole states [1]. This splitting depends in turn on the direction of the in-plane wavevector relative to the orientation of the strain [22] which results in the highly anisotropic spin-dependent deformation of the Fermi contours displayed in Fig. 1(a).

In Fig. 4 we show similar data taken on the same AD region ($a = 600 \text{ nm}$) as in Fig. 3, but here the MR traces are taken at different values of hole density while the strain is kept fixed at 5.7×10^{-4} . Two strong MR peaks A and B are observed whose positions move to higher fields with increasing density. As seen in Fig. 4, there is again good quantitative agreement between the experimental data and the calculated positions of these MR peaks.

Data for the AD region with period 750 nm and with current along $[01\bar{1}]$ are shown in Figs. 3(b) and (b'). The

MR traces are overall qualitatively similar to those for the 600 nm period AD region in that they show two strong peaks, labelled A and B, which move in opposite directions in field with increasing strain. The positions of these peaks are in good agreement with the results of the calculations, although peak B is observed at somewhat lower field values than expected.

In Figs. 3(c) and (c') we show the data for the 750 nm period region with current along $[2\bar{3}3]$. Again we observe two prominent peaks, which we label A and B, but here the peaks are seen at very low field values and their positions are essentially independent of strain. Note that in this case the MR data probe k_F along $[2\bar{3}3]$ for the HHh and HHI subbands. As seen in Fig. 1(a), in the strain range that our experiments probe (4.5 to 6.9×10^{-4}), k_F of the HHh and HHI bands along $[2\bar{3}3]$ are close in size and are both smaller than k_F along $[01\bar{1}]$. This is reflected in the B_P curves shown in Fig. 3(c') which predict two essentially overlapping MR peaks that occur at small fields and whose positions are nearly independent of strain. It is therefore likely that our observed peak A corresponds to the commensurate orbits of both HHh and HHI bands, and peak B is the low-field peak commonly observed in AD lattices with soft potentials [14].

We also took data on another sample from the same wafer and with similar AD lattices, but not mounted on a piezo-actuator so that it is strain-free. Our results for this sample are similar to those reported by Zitzlsperger *et al.* [18] where MR peaks in an un-strained 2DHS with AD lattices were studied, and corroborate our conclusions. The low-field MR traces for our un-strained sample show a peak at a magnetic field whose position lies between the two B_P theoretically expected for the HHh and HHI contours. Evidently we cannot resolve the two commensurability peaks for the HHh and HHI bands at zero strain

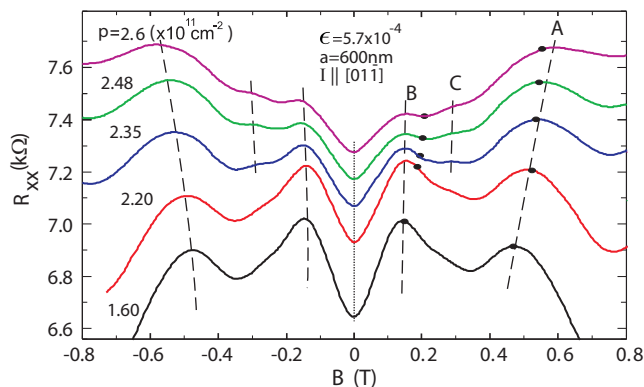


FIG. 4: (Color online) Low-field MR traces for the 600 nm AD region for different densities at $\epsilon = 5.7 \times 10^{-4}$. Traces are offset, except for the bottom one. Theoretically expected MR peak positions are shown by filled circles on each trace.

where the two peaks are theoretically expected to be close to each other. Given the relatively large width of the MR peaks, this is not surprising. More revealing is the observation that the MR traces for the AD lattices patterned on the two Hall bar arms (along $[233]$ and $[01\bar{1}]$) of our strain-free sample are fairly similar. This implies that the Fermi contours are nearly isotropic at zero strain, consistent with the calculations (see Fig. 1(a)). In contrast, the data in Figs. 3(b,b') and 3(c,c') are clearly very different, reflecting the strong anisotropy of the Fermi contours at large strains.

While the overall agreement between the experimental data and calculations shown in Figs. 3 and 4 is good [26], there are some puzzles. First, the positions of the lower MR peak (peak B) in most of the experimental data are somewhat smaller than expected from the calculations. Second, the variation (slope) of the peak A position with strain is slightly faster than the calculations predict. We do not have a clear explanation for these discrepancies. They might be arising from the simplifications of theoretical model that is based on the properties of the un-patterned 2DHS. It is also possible that the cyclotron orbits are slightly distorted in the AD lattice regions (compared to the un-patterned regions) because of the non-ideal (e.g., not perfectly abrupt) potentials of the ADs [14]. Third, for current along $[01\bar{1}]$, some of the experimental MR traces exhibit a weak peak (labelled C) between peaks A and B (see Figs. 3 and 4). Note in Fig. 1(a) that in the strain range of our measurements, k_F along $[233]$ for the Hh and Hl bands are quite close to each other. It is tempting to associate this peak C with a magnetic-breakdown-like phenomenon where the hole trajectory switches from the Hh to Hl orbit when these orbits come close to each other in k -space. Sup-

porting such a conjecture is the fact that, in the strain and density range where we observe peak C, the Fourier power spectra of the SdH oscillations also show a peak at the frequency $f_{\text{ave}} = (f_+ + f_-)/2$ (see Fig. 2 inset). Such a peak could indicate a magnetic-breakdown [27].

Despite these puzzles, our results provide strong evidence that we are probing the ballistic transport in individual spin-subbands. They also show that we can tune the anisotropy of the Fermi contours, and therefore the cyclotron orbit trajectories, via the application of strain. Such tuning may find applications in ballistic spintronic devices, e.g., it could facilitate the separation of carriers in different spin subbands in magnetic focusing devices [9].

We thank the DOE, NSF, and ARO for support and S. Misra and B. Habib for useful advice.

-
- [1] R. Winkler, *Spin-Orbit Coupling Effects in Two-Dimensional Electron and Hole Systems* (Springer, Berlin, 2003).
 - [2] S. Datta and B. Das, *Appl. Phys. Lett.* **56**, 665 (1990).
 - [3] For reviews, see e.g., G.A. Prinz, *Physics Today* **48**, 58 (1995); S.A. Wolf *et al.*, *Science* **294**, 1488 (2001); I. Žutić *et al.*, *Rev. Mod. Phys.* **76**, 323 (2004).
 - [4] A.F. Morpurgo *et al.*, *Phys. Rev. Lett.* **80**, 1050 (1998).
 - [5] J.B. Yau *et al.*, *Phys. Rev. Lett.* **88**, 146801 (2002).
 - [6] T. Koga *et al.*, *Phys. Rev. B* **70**, 161302(R) (2004).
 - [7] H. Engels *et al.*, *cond-mat/0603306* (2006).
 - [8] J.P. Lu *et al.*, *Phys. Rev. Lett.* **81**, 1282 (1998); J.P. Lu *et al.*, *Phys. Rev. B* **60**, 13776 (1999).
 - [9] L.P. Rokhinson *et al.*, *Phys. Rev. Lett.* **93**, 146601 (2004).
 - [10] K.I. Kolokolov *et al.*, *Phys. Rev. B* **59**, 7537 (1999).
 - [11] B. Habib *et al.*, *Appl. Phys. Lett.* **91**, 012107 (2007).
 - [12] D. Weiss *et al.*, *Phys. Rev. Lett.* **66**, 2790 (1991).
 - [13] A. Lorke *et al.*, *Phys. Rev. B* **44**, 3447 (1991).
 - [14] R. Fleischmann *et al.*, *Phys. Rev. Lett.* **68**, 1367 (1992).
 - [15] K. Tsukagoshi *et al.*, *Phys. Rev. B* **52**, 8344 (1995).
 - [16] W. Lu, *Phys. Rev. B* **54**, 8049 (1996).
 - [17] O. Gunawan *et al.*, *Phys. Rev. B* **75**, 081304(R) (2007).
 - [18] M. Zitzlsperger *et al.*, *Europhys. Lett.* **61**, 382 (2003).
 - [19] M. Shayegan *et al.*, *Appl. Phys. Lett.* **83**, 5235 (2003).
 - [20] B. Habib *et al.*, *Phys. Rev. B* **75**, 153304 (2007).
 - [21] G.L. Bir and G.E. Pikus, *Symmetry and Strain-induced Effects in Semiconductors* (Wiley, New York, 1974).
 - [22] H.R. Trebin *et al.*, *Phys. Rev. B* **20**, 686 (1979).
 - [23] R. Winkler and U. Rössler, *Phys. Rev. B* **48**, 8918 (1993).
 - [24] S.J. Papadakis *et al.*, *Physica E* **9**, 31 (2001).
 - [25] R. Winkler *et al.*, *Phys. Rev. Lett.* **84**, 713 (2000).
 - [26] Data for other densities and current direction, not shown here, exhibit equally good agreement with calculations.
 - [27] S. Keppeler and R. Winkler, *Phys. Rev. Lett.* **88**, 046401 (2002).